Development of an Analytical Model of Wing Rock for Slender Delta Wings

J. M. Elzebda,* A. H. Nayfeh,† and D. T. Mook‡
Virginia Polytechnic Institute and State University, Blacksburg, Virginia

Three analytical models of the subsonic wing-rock phenomenon for slender delta wings mounted on free-to-roll stings are compared. The first model was developed earlier by other investigators, the second is a version of the first model that has been modified in the present paper, and the third was developed in an earlier paper by the authors. The differences among the three models lie in the assumed nonlinear form of the roll moment as a function of the roll angle and its derivative. The numerical values of the coefficients in the moment expressions are obtained by fitting them to moments obtained in an earlier numerical simulation. It is shown that the original model, which contains only quadratic terms, does not predict roll divergence. The model is modified by the addition of a cubic term, and the modified version does predict roll divergence. An asymptotic approximation to the solution of the equation of motion is obtained for the modified model, and it is shown that the solution reduces to the one given when the cubic term is dropped. Finally, the two models are compared with a third model developed earlier by the authors. The periods and amplitudes predicted by the asymptotic analysis for all three models are in close agreement with the numerical simulations, which were found in an earlier work to be in good agreement with experimental data. It appears that the authors' model is slightly more accurate and easier to analyze than either the earliest model or the modified version of that model.

Introduction

SUBSONIC wing rock of slender delta wings has been the subject of several articles. As a step toward providing some basic understanding of the phenomenon, a series of two wind-tunnel experiments[1,2] were performed. In these experiments, slender delta wings were mounted on free-to-roll stings. The angle of attack was increased until the wing spontaneously began to oscillate. Subsequently, Konstadinopoulos et al.[3] developed a numerical simulation of this experiment, and from this simulation Nayfeh et al.[4] developed an analytical model. At about the same time, Hsu and Lan[5] also developed an analytical model. There are some significant differences between these two analytical models, and the purpose of the present paper is to provide a critical comparison of the two.

Analytical Models

Hsu and Lan[5] and Nayfeh et al.[4] worked with the following equation of motion:

$$\ddot{\phi} = \frac{\rho U_\infty^2 Sb}{2I_{xx}} C_l + D\dot{\phi} \tag{1}$$

where ϕ is the roll angle, ρ is the density of air, U_∞ is the speed of the freestream, S is the plan form area, b is the chord, C_l is the roll-moment coefficient, and I_{xx} is the mass moment of inertia of the wing around the midspan axis. The last term models the effects of (viscous) damping in the bearing; it was not included in the analysis by Hsu and Lan. The major difference between the two models is in the assumed form of C_l.

Model of Hsu and Lan

Hsu and Lan proposed the following:

$$\ddot{\phi} = L_0 + \sin\alpha L_\beta \phi + L_{p0}\dot{\phi} + L_{p\beta}\sin\alpha|\phi|\dot{\phi} + L_{pp}|\dot{\phi}|\dot{\phi} \tag{2}$$

where L_0, L_β, Lp_0, Lp_β, and L_{pp} are constants and α is the angle between the freestream and the axis of rotation of the wing (called angle of attack in the following; see Fig. 1). They took L_0 to be zero in all of their results, and we do the same here. To investigate the properties of the solution of Eq. (1), it is useful to have numerical values for the constants on the right-hand side. Hsu and Lan did not provide these constants. As a result, we turn to the numerical simulation of Konstadinopoulos et al.[3]

One of the benefits of having such a simulation is that the aerodynamic roll moment is predicted as a function of time. The numerical simulation of Ref. 3 accurately imitated the behavior of the wing observed in the wind-tunnel tests of Nguyen et al.[1] and Levin and Katz,[2] giving close estimates of both the amplitude and the period of the limit-cycle motion; thus, it is likely that the numerically predicted roll moment is also accurate. These numerical simulations were conducted using the delta wing shown in Fig. 1 for the case where $d = 0$.

Following Hsu and Lan, we write the (dimensionless) roll moment around the midspan chord as

$$C_l = a_1\phi + a_2\dot{\phi} + a_3|\phi|\dot{\phi} + a_4|\dot{\phi}|\dot{\phi} \tag{3}$$

Next, we obtain numerical values for the a_i by fitting this expression to the numerically obtained moment using a least-

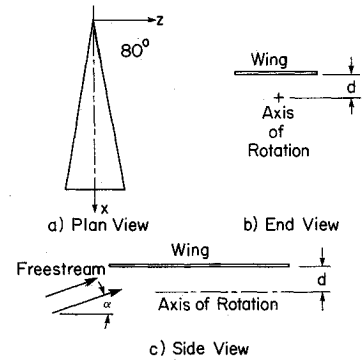

Fig. 1 Schematic representation of a delta wing on a free-to-roll sting; $d \neq 0$ corresponds to the experiments of Nguyen et al.[1] and $d = 0$ corresponds to the experiments of Levin and Katz.[2]

Received Sept. 27, 1988; revision received Jan. 9, 1989.

*Assistant Professor.
†University Distinguished Professor. Member AIAA.
‡Professor. Member AIAA.

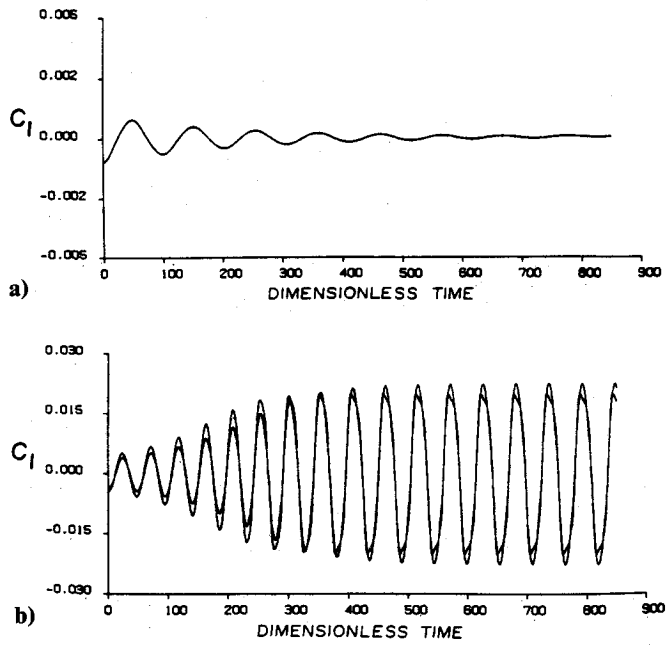

Fig. 2 Roll-moment coefficient as a function of time: a) $\alpha = 15$ deg (a stable case), b) $\alpha = 25$ deg (an unstable case). Each part contains the values of c_l obtained from both the numerical simulation and Eq. (3).

Table 1 Coefficients in Eq. (3) for different angles of attack

α, deg	a_1	a_2	a_3	a_4
15.0	−0.0106857	−0.02192166	0.11961137	−0.3317292
21.5	−0.03518571	0.01595784	−0.0688440	0.05353120
22.5	−0.03557399	0.02891174	−0.10454088	−0.02906233
25.0	−0.03881275	0.065991965	−0.1942874	−0.27968228

Table 2 Coefficients in Eq. (4) for different angles of attack

α, deg	$\omega^2 = \sin\alpha L_\beta$	$\mu = Lp_o$	$b_1 = \sin\alpha L_{p\beta}$	$b_2 = L_{pp}$
15.0	0.0037805	−0.0087556	0.04231681	−0.11736108
21.5	0.0124482	+0.00464566	−0.02435604	+0.01893858
22.5	0.01258557	+0.00923058	−0.03698508	−0.01028184
25.0	0.01373140	+0.0223470	−0.06873613	−0.09894762

squares criterion. There is a set of the a_i for each angle of attack α. Some examples are given in Table 1.

In Fig. 2, both the moment coefficient from the numerical simulation and the moment coefficient given by Eq. (3) and the constants in Table 1 are shown as functions of time. The results were obtained by releasing the wing from rest at an initial displacement of 5 deg. In Fig. 2a, the angle of attack is 15 deg, and in Fig. 2b, the angle of attack is 25 deg. Clearly, the smaller angle of attack is stable whereas the larger is unstable. The results from Eq. (3) fit the data (i.e., numerically obtained results) better at the smaller angle of attack. One can clearly see differences at the higher angle of attack.

Substituting Eq. (3) into Eq. (1), and rearranging the result, we obtain

$$\ddot{\phi} + \omega^2\phi = \mu\dot{\phi} + b_1|\phi|\dot{\phi} + b^2|\dot{\phi}|\dot{\phi} \tag{4a}$$

where

$$\omega^2 = -Ca_1 = -\sin\alpha_s L_\beta \tag{4b}$$

$$\mu = C_2 - D = L_{p0} - D \tag{4c}$$

$$b_1 = Ca_3 = \sin\alpha L_{p\beta} \tag{4d}$$

$$b_2 = Ca_4 = L_{pp} \tag{4e}$$

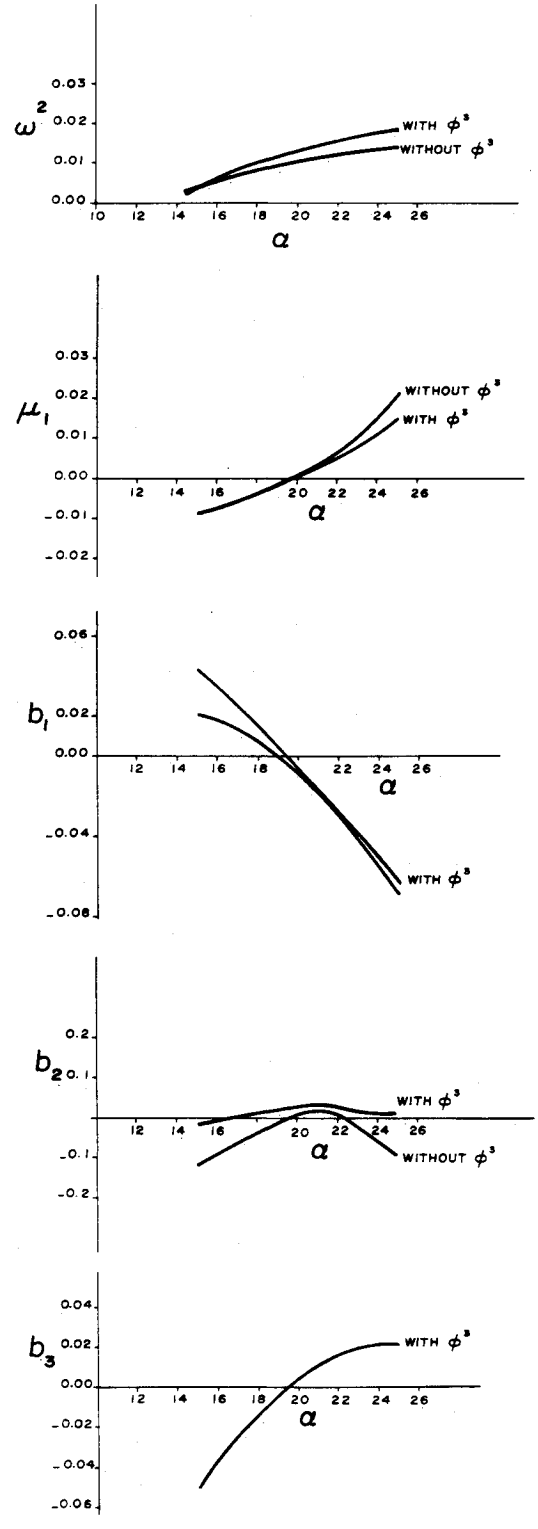

Fig. 3 The coefficients of Eq. (4) (without ϕ^3), and of Eq. (11) (with ϕ^3) as a function of angle of attack.

$$C = \frac{\rho U_\infty^2 Sb}{I_{xx}} = 0.354 \qquad D = 0.001 \tag{4f}$$

The values of C and D were also used in the numerical simulation. The numerical values of the coefficients in Eq. (4) are given in Table 2. These coefficients are plotted as functions of angle of attack in Fig. 3. In Fig. 3, there are two sets of curves, one labeled "with ϕ^3" and the other labeled "without ϕ^3." For now we are concerned only with the curves labeled without ϕ^3. Subsequently, we will modify Eq. (4), and

the curves labeled with ϕ^3 correspond to the modification. The point where μ is zero corresponds to the onset of wing rock. Here the critical angle of attack is between 19–20 deg.

Next, we consider the phase plane corresponding to Eq. (4). To write Eq. (4) as a system of two first-order equations, we let

$$y_1 = \phi, \qquad y_2 = \dot{\phi}$$

Then

$$\dot{y}_1 = y_2 \tag{5a}$$

$$\dot{y}_2 = -\omega^2 y_1 + \mu y_2 + b_1 |y_1| y_2 + b_2 |y_2| y_2 \tag{5b}$$

The equilibrium positions of the motion correspond to

$$\dot{y}_1 = 0, \qquad \dot{y}_2 = 0 \tag{6}$$

The only solution is

$$y_1 = y_2 = 0 \tag{7}$$

As we will see in the following, the fact that there is only one equilibrium position is a serious shortcoming of this model.

To investigate the stability of the equilibrium point at the origin, we introduce a small perturbation in y_1 and y_2 given by the functions u_1 and u_2, respectively. Then it follows from Eq. (5) that

$$\dot{u}_1 = u_2 \tag{8a}$$

$$\dot{u}_2 = -\omega^2 u_1 + \mu u_2 \tag{8b}$$

when all of the nonlinear terms are ignored. The eigenvalues of Eqs. (8) are

$$\lambda_1, \lambda_2 = \frac{1}{2}\mu \pm \sqrt{\mu^2 - 4\omega^2} \tag{9}$$

Generally, $|2\omega| > |\mu|$ (this is true in the present example for the range of $15 \le \alpha \le 25$ deg); consequently, λ_1 and λ_2 are complex conjugates and the stability of this equilibrium point (the origin) is determined by the sign of μ. As we already noted, μ changes sign at approximately 19.5 deg. For $\alpha > 19.5$ deg, the origin is an unstable focus; for $\alpha < 19.5$ deg, the origin is a stable focus; and for $\alpha = 19.5$ deg, the origin is a center, and often called a Hopf bifurcation point.

The entire planes for $\alpha = 15$ and 25 deg are shown in Figs. 4a and 4b, respectively. These planes were constructed by numerically integrating Eqs. (5) for the two sets of constants corresponding to 15 and 25 deg given in Table 2. We note that, no matter how large the initial conditions, this model does not predict divergence (i.e., continuous rolling in one direction instead of oscillations). Yet divergence has been observed[6] for slender delta wings, such as the one considered in the present paper (Fig. 1). For the model to predict divergence, it must have more than one equilibrium position.

Modified Model of Hsu and Lan

Next, we consider the effect of modifying the model of Hsu and Lan by adding a cubic term to the expression for the moment [Eq. (3)], so that

$$C_l = a_1\phi + a_2\dot{\phi} + a_3|\phi|\dot{\phi} + a_4|\dot{\phi}|\dot{\phi} + a_5\phi^3 \tag{10}$$

The values of the a_i were obtained by fitting Eq. (10) to the same numerical data and are given in Table 3.

In Fig. 5, both the moment obtained from the numerical simulation, as well as the moment given by Eq. (10), and the numerical values of the a_i in Table 3 are shown as functions of time. Comparing Fig. 2 with Fig. 5, we note that the addition of the cubic term greatly enhanced the agreement between the two moments, especially in the limit-cycle motion. Comparing Table 1 with Table 3, we note that the addition of the cubic term caused all of the coefficients to change and that the coefficients of the nonlinear terms changed more than those of the linear terms.

Substituting Eq. (10) into Eq. (1) leads to

$$\ddot{\phi} + \omega^2\phi = \mu\dot{\phi} + b_1|\phi|\dot{\phi} + b_2|\dot{\phi}|\dot{\phi} + b_3\phi^3 \tag{11a}$$

where ω^2, μ, b_1, and b_2 are defined as they were in Eqs. (4), and

$$b_3 = Ca_5 \tag{11b}$$

Both C and D retain the values used in the numerical simula-

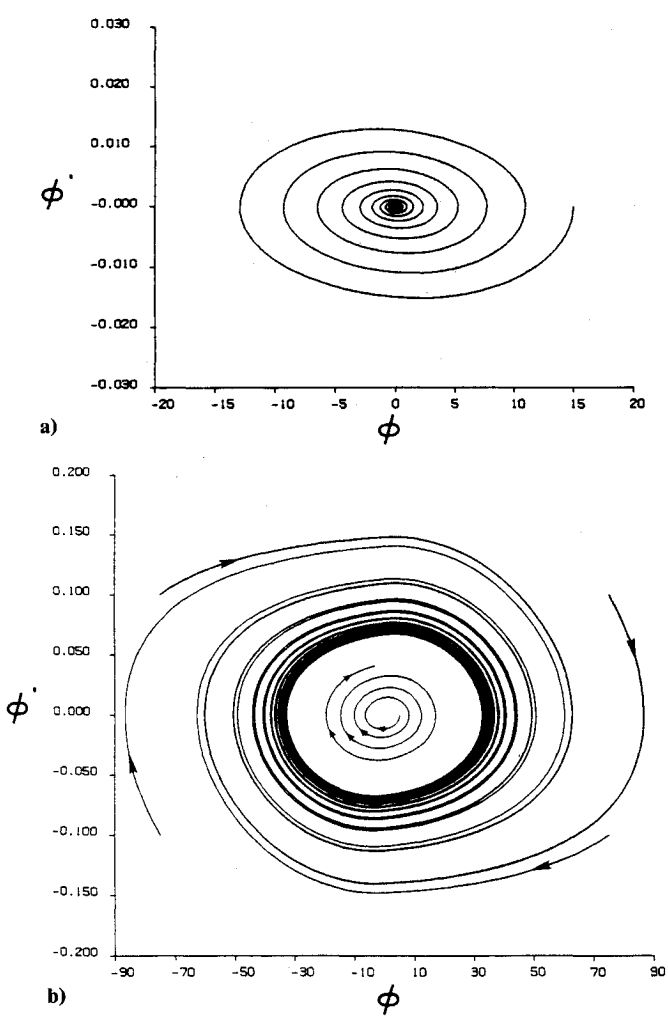

Fig. 4 Phase planes obtained by numerical integration of Eq. (5): a) $\alpha = 15$ deg; and b) $\alpha = 25$ deg.

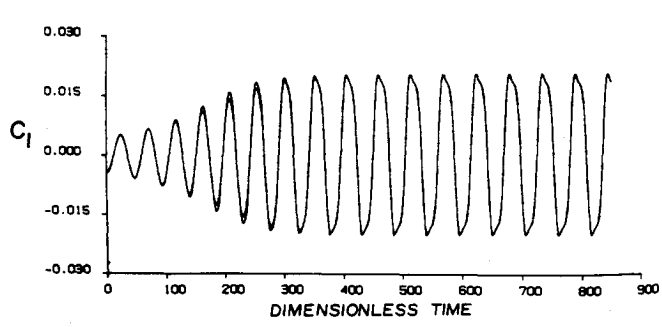

Fig. 5 Roll-mount coefficient as a function of time for $\alpha = 25$ deg. Plotted are the values of c_l obtained from both the numerical simulation and Eq. (10).

Table 3 Coefficients in Eq. (10) of different angles of attack

α, deg	a_1	a_2	a_3	a_4	a_5
15.0	−0.0102590	−0.0214337	0.05711631	−0.0619253	−0.14664512
21.5	−0.04177563	0.01461574	−0.06732727	0.08415139	0.04606465
22.5	−0.04569571	0.0235172	−0.09944902	0.06890047	0.05315907
25.0	−0.0525606	0.04568407	−0.17652355	0.0269855	0.06063813

Table 4 Coefficients in Eq. (11) for different angles of attack

α, deg	ω^2	μ	b_1	b_2	b_3
15.0	0.00362949	−0.00858295	0.02020694	−0.0219083	−0.051880962
21.5	0.01477963	0.004170843	−0.02381943	0.02977157	0.016297021
22.5	0.016166495	0.00732005	−0.03518365	0.02437601	0.01880692
25.0	0.01859521	0.015162375	−0.06245153	0.00954708	0.02145291

Table 5 Amplitudes and periods of the limit-cycle motions predicted by the three analytical models for different angles of attack

	Amplitude			Period, $\frac{T\omega}{2\pi}$		
	Model of Nayfeh et al.	Model of Hsu and Lan		Model of Nayfeh et al.	Model of Hsu and Lan	
α, deg		Without ϕ^3	With ϕ^3		Without ϕ^3	With ϕ^3
15.0	—	—	—	—	—	—
21.5	28.79	31.15	33.96	1.11	1.00	1.145
22.5	31.49	31.70	34.09	1.15	1.00	1.154
25.0	32.94	32.82	34.20	1.18	1.00	1.154

tion. The values of the coefficients in Eq. (11) are given in Table 4.

These coefficients are plotted in Fig. 3 and they correspond to the set of curves labeled with ϕ^3. We note that the addition of the cubic term did not significantly affect the predicted critical angle of attack.

Next, we consider the phase plane corresponding to Eq. (11). Following the same procedure as before, we rewrite Eq. (11) as a system of two first-order equations

$$\dot{y}_1 = y_2 \tag{12a}$$

$$\dot{y}_2 = -\omega^2 y_1 + \mu y_2 + b_1|y_1|y_2 + b_2|y_2|y_2 + b_3 y_1^3 \tag{12b}$$

The equilibrium positions correspond to

$$y_1 = y_2 = 0 \tag{13}$$

$$y_1 = \pm\frac{\omega}{\sqrt{b_3}}, \qquad y_2 = 0 \tag{14}$$

Referring to Fig. 3e, we note that b_3 is negative at low angles of attack and positive at high angles of attack, and it appears to change sign at the critical angle; thus, below the critical angle there is only one equilibrium point, and the addition of the cubic term to the moment expression, Eq. (10), appears to have little effect. However, at the critical angle of attack, two additional equilibrium points form far from the origin. As the angle of attack increases, these new equilibrium points move inward (b_3 increases). Thus, for supercritical angles of attack, the addition of the cubic term to the moment expression appears to have a profound effect.

To investigate the stability of the equilibrium points, we again introduce small perturbations:

$$y_1 = y_{10} + u_1 \tag{15a}$$

$$y_2 = u_2 \tag{15b}$$

where y_{10} is the coordinate of an equilibrium position, i.e., Eq. (13) and (14) (y_{20} is zero for all points). Substituting Eqs. (15) into Eqs. (12) and neglecting nonlinear terms in u_1 and u_2 leads to

$$\dot{u}_1 = u_2 \tag{15c}$$

$$\dot{u}_2 = (3b_3 y_{10}^2 - \omega^2)u_1 + (\mu + b_1|y_{10}|)u_2 \tag{15d}$$

The eigenvalues of this system are

$$\lambda_1, \lambda_2 = \frac{1}{2}\left[\mu + b_1|y_{10}| \pm \sqrt{12b_3 y_{10}^2 - 4\omega^2 + (\mu + b_1|y_{10}|)^2}\right] \tag{16}$$

For $y_{10} = 0$, Eq. (16) reduces to Eq. (9) and we find that the origin changes from stable to unstable near $\alpha = 19.5$ deg as before. We note that simultaneously two additional equilibrium points develop at

$$y_1 = \pm\frac{\omega}{\sqrt{b_3}}$$

and for the new equilibrium points, Eq. (14) reduces to

$$\lambda_1, \lambda_2 = \frac{1}{2}\left[\mu + \frac{b_1\omega}{\sqrt{b_3}} \pm \sqrt{8\omega^2 + \left(\mu + \frac{b_1\omega}{\sqrt{b_3}}\right)^2}\right] \tag{17}$$

Both λ_1 and λ_2 are real, and regardless of the sign of

$$\mu + \frac{b_1\omega}{\sqrt{b_3}}$$

one is positive and one is negative. Thus, both of these equilibrium points are unstable saddle points.

The phase planes for angles of attack of 15 and 25 deg are shown in Fig. 6. These planes were obtained numerically by integrating Eqs. (12). The results for the 15-deg angle of attack are shown in Fig. 6a and are nearly the same as those in Fig. 4a. The results for the 25-deg angle of attack are shown in Fig. 6b. These results have some features in common with the results shown in Fig. 4b, but there are also some profound

differences. The remainder of the discussion in this section applies to the 25-deg angle of attack.

There is a limit cycle in both Figs. 4b and 6b, and the two limit cycles have nearly the same amplitude and period. However, in Fig. 4b all initial conditions lead to the one limit cycle, but in Fig. 6b some initial conditions lead to the limit cycle and some (such as those labeled A) lead to roll divergence (i.e., continuous rolling instead of oscillatory motion). In fact, the boundaries between the initial conditions leading to divergence and those leading to oscillations are clearly evident. Roll divergence has been observed for 80-deg delta wings.[6] Hence, the evidence strongly suggests that cubic terms must be included in the moment expression.

We can gain some additional insight into the character of the solutions of Eqs. (4) and (11) by obtaining an asymptotic approximation to the solution. This is done in the next section.

Asymptotic Analysis of the Equation of Motion

In this section, we construct an approximate solution of Eq. (11) using the method of multiple scales (see Nayfeh[7,8] and Nayfeh and Mook[9]). Equation (4a) can be regarded as a special case ($b_3 = 0$). As a bookkeeping aid in the analysis, we introduce a parameter ϵ, which can serve as a measure of the strength of the nonlinearity, and then rewrite Eq. (11) as

$$\ddot{\phi} + \omega^2\phi = \epsilon(2\beta_1\dot{\phi} + \beta_2|\phi|\dot{\phi} + \beta_3|\dot{\phi}|\dot{\phi} + \beta_4\phi^3) \tag{18a}$$

where

$$2\epsilon\beta_1 = \mu, \qquad \epsilon\beta_2 = b_1, \qquad \epsilon\beta_3 = b_2, \qquad \epsilon\beta_4 = b_3 \tag{18b}$$

Next, we assume that the solution of Eq. (18a) can be approximated, for small ϵ, by an expansion in the form

$$\phi \simeq \phi_0(T_0, T_1) + \epsilon\phi_1(T_0, T_1) \tag{19}$$

where $T_0 = t$ and $T_1 = \epsilon t$ are the so-called fast and slow scales, respectively. To include more terms in the expansion, one must also include more scales. Through the use of the chain rule, ordinary derivatives with respect to t now become expansions in terms of partial derivatives with respect to the fast and slow scales:

$$\frac{d\phi}{dt} = D_0\phi_0 + \epsilon(D_1\phi_0 + D_0\phi_1) + \ldots \tag{20a}$$

$$\frac{d^2\phi}{dt^2} = D_0^2\phi_0 + \epsilon(2D_0D_1\phi_0 + D_0^2\phi_1) + \ldots \tag{20b}$$

where

$$D_0 = \frac{\partial}{\partial T_0} \text{ and } D_1 = \frac{\partial}{\partial T_1}$$

In Eqs. (20), squares and higher powers of ϵ were ignored in order to make Eqs. (20) consistent with Eq. (19).

Substituting Eqs. (20) and (19) into Eq. (18a), ignoring squares and higher powers of ϵ and setting the coefficients of ϵ^0, and ϵ equal to zero independently, we obtain

$$D_0^2\phi_0 + \omega^2\phi_0 = 0 \tag{21}$$

$$D_0^2\phi_1 + \omega^2\phi_1 = -2D_0D_1\phi_0 + 2\beta_1D_0\phi_0 + \beta_2|\phi_0|D_0\phi_0 + \beta_3|D_0\phi_0|D_0\phi_0 + \beta_4\phi_0^3 \tag{22}$$

The solution of Eq. (21) can be written in the form

$$\phi_0 = a(T_1)\cos[\omega T_0 + \Theta(T_1)] = a\cos\psi \tag{23}$$

where a and Θ are real functions of the slow scale T_1 [Eq. (21)] is a partial differential equation in which functions of T_1 are

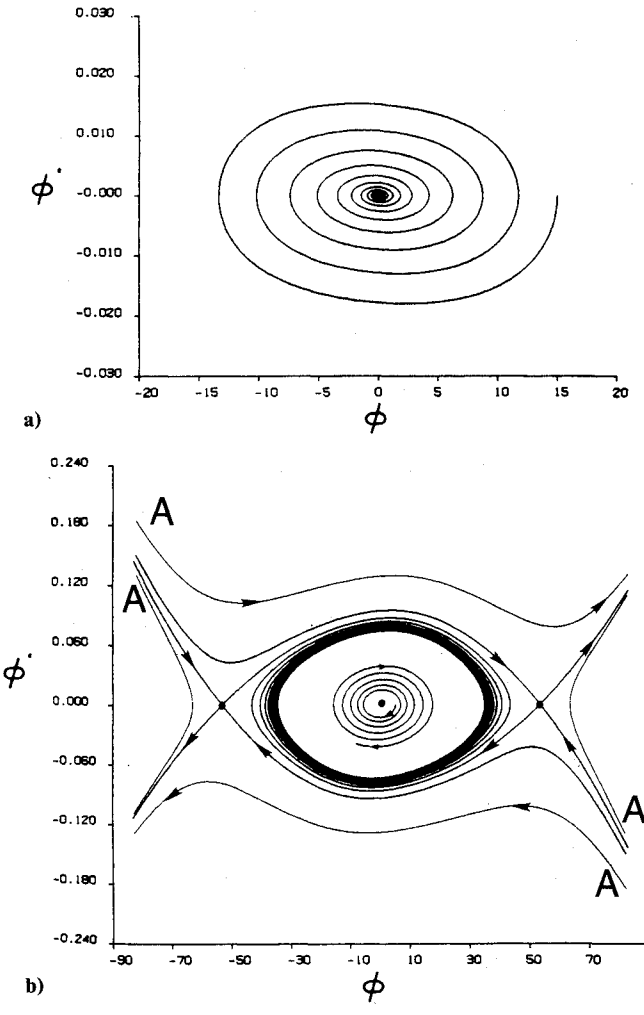

Fig. 6 Phase planes obtained by numerical integration of Eq. (12): a) $\alpha = 15$ deg; b) $\alpha = 25$ deg.

treated as constants]. At this point, a and Θ are arbitrary functions; they will be determined later when the secular terms are eliminated from ϕ_1.

Next, we substitute Eq. (23) into Eq. (22) and obtain

$$D_0^2\phi_1 + \omega^2\phi_1 = 2\omega(a'\sin\psi + a\Theta'\cos\psi) - 2\beta_1\omega a\sin\psi - \beta_2\omega a^2|\cos\psi|\sin\psi - \beta_3\omega^2a^2|\sin\psi|\sin\psi + \frac{\beta_4a^2}{4}(3\cos\psi + \cos3\psi) \tag{24}$$

where the prime denotes the derivative with respect to the argument. Both $|\cos\psi|\sin\psi$ and $|\sin\psi|\sin\psi$ are periodic functions of the fast scale T_0 and can be expanded in Fourier series as

$$|\cos\psi|\sin\psi = \frac{4}{3\pi}\sin\psi + \ldots \tag{25a}$$

$$|\sin\psi|\sin\psi = \frac{8}{3\pi}\sin\psi + \ldots \tag{25b}$$

After substituting Eqs. (25) into Eq. (24) and rearranging the result, one obtains

$$D_0^2\phi_1 + \omega^2\phi_1 = \left(2\omega a' - 2\omega\beta_1a - \frac{4\beta_2\omega}{3\pi}a^2 - \frac{8\beta_3\omega^2}{3\pi}a^2\right)\sin\psi + 2\omega a\Theta' + \frac{3\beta_4a^3}{4}\cos\psi + \ldots \tag{26}$$

Because $\sin\psi$ and $\cos\psi$ are solutions of the corresponding homogeneous equation, any particular solution for ϕ_1 will contain terms having the factors $T_0 \sin\psi$ and $T_0 \cos\psi$. These terms are the so-called secular terms. Secular terms render the approximation [Eq. (19)] invalid as $t \to \infty$, because eventually $\epsilon\phi_1$ will be larger than ϕ_0 instead of being a small correction to ϕ_0.

To eliminate the secular terms from ϕ_1, one must set the coefficients of $\cos\psi$ and $\sin\psi$ in Eq. (26) equal to zero; that is,

$$a' - \beta_1 a - \frac{2}{3\pi}(\beta_2 + 2\beta_3\omega)a^2 = 0 \tag{27}$$

$$\Theta' + \frac{3\beta_4}{8\omega} a^2 = 0 \tag{28}$$

After recalling the definitions of the β_i, Eq. (18b), and T_1, we can rewrite Eq. (27) as follows:

$$\frac{da}{dt} = \frac{\mu}{2} a + \frac{2}{3\pi}(b_1 + 2\omega b_2)a^2 \tag{29}$$

Equation (29) can be integrated to yield the following expression for the amplitude of the motion:

$$a = \frac{\exp\left(\frac{\mu}{2} t\right)}{K - R \exp\left(\frac{\mu}{2} t\right)} \tag{30a}$$

where

$$R = \frac{4(b_1 + 2\omega b_2)}{3\pi\mu} \qquad K = (1 + Ra_0)/a_0 \tag{30b}$$

and a_0 is a constant of integration, the initial amplitude.

Substituting Eq. (30a) into Eq. (28), replacing β_4 and T_1, and then integrating the result leads to

$$\Theta = \Theta_0 - \frac{3b_3}{4\mu\omega R}\left\{ \frac{\exp\left(\frac{\mu}{2} t\right)}{K - R \exp\left(\frac{\mu}{2} t\right)} + \frac{1}{R} \ln\left[K - R \exp\left(\frac{\mu}{2} t\right)\right]\right\} \tag{31}$$

where Θ_0 is another constant of integration; R and K are given above in Eq. (30b).

The first approximation to the solution of Eq. (11) is

$$\phi \simeq a \cos(\omega t + \Theta) \tag{32}$$

where a is given by Eq. (30a) and Θ is given by Eq. (31).

Next, we consider the behavior of ϕ as t becomes large. It follows from Eqs. (30a), (31), and (32) that

$$\phi \to 0 \qquad \text{if } \mu < 0 \tag{33a}$$

(motion decays, wing rock does not occur); and

$$\phi \to -\frac{1}{R} \cos\left[\left(\omega - \frac{3b_3}{8\omega R^2}\right)t + \Theta_0 + \frac{3b_3}{2\mu\omega R^2}(1 - \ln R)\right], \tag{33b}$$

if $\mu > 0$ (limit-cycle motion develops, wing rock occurs).

The amplitude of the limit cycle is

$$a_{lc} = \frac{1}{R} = \frac{3\pi\mu}{4b_1 + 8\omega b_2} \tag{34}$$

To this approximation, the amplitude is not affected by the cubic term (b_3 is the coefficient of the cubic term). In fact, when Eq. (34) is rewritten in terms of the original coefficients, Eqs. (4b–4e), the result is

$$a_{lc} = \frac{3\pi L p_0}{4(\sin\alpha L_{p\beta} + 2L_{pp}\omega)} \tag{35}$$

which agrees with the amplitude of the limit-cycle motion obtained by Hsu and Lan. The period of the limit-cycle motion is given by

$$T = \frac{2\pi}{\omega - \frac{3b_3}{8\omega R^2}} \simeq \frac{2\pi}{\omega}\left[1 + \frac{27\pi^2\mu^2 b_3}{128\omega^2(b_1 + 2\omega b_2)^2}\right] \tag{36}$$

The period of the motion is affected by the cubic term. If b_3 is zero, then

$$T \simeq \frac{2\pi}{\omega} = \frac{2\pi}{\sqrt{-\sin\alpha_s L_\beta}} \tag{37}$$

which also agrees with the result obtained by Hsu and Lan.

Model of Nayfeh, Elzebda, and Mook

The authors also developed an analytical model of wing rock.[4] The equation of motion was the same as Eq. (1). However, instead of expressing the roll-moment coefficient as Hsu and Lan did in Eq. (3), the authors used the following form:

$$C_l = a_1\phi + a_2\dot{\phi} + a_3\phi^3 + a_4\phi^2\dot{\phi} + a_5\dot{\phi}^2\phi \tag{38}$$

which leads to a governing equation of the form

$$\ddot{\phi} + \omega^2\phi = \mu_1\dot{\phi} + b_1\phi^3 + \mu_2\phi^2\dot{\phi} + b_2\phi\dot{\phi}^2 \tag{39a}$$

where

$$\omega^2 = -Ca_1, \qquad \mu_1 = Ca_2 - D, \qquad b_1 = Ca_3 \tag{39b}$$

$$\mu_2 = Ca_4, \qquad b_2 = Ca_5 \tag{39c}$$

where C and D are given in Eq. (4f). The characteristics of the solutions of Eqs. (11) and (39) are quite similar. Both predict stable limit cycles and divergence above the critical angle of attack. An asymptotic analysis of Eq. (39a) yields the following expressions for the amplitude and period of the limit cycle:

$$a_{lc} = 2(-\mu_1/\mu_2)^{1/2} \tag{40}$$

$$T = \frac{2\pi}{\omega}\left[1 - \frac{\mu_1(3b_1 + \omega^2 b_2)}{2\mu_2\omega^2}\right] \tag{41}$$

The coefficients in Eq. (38) were obtained in precisely the same manner used to obtain those in Eqs. (3) and (10), and the same data (i.e., numerical results) were used for both equations. The coefficients are given in Ref. 4. Both Eqs. (38) and (10) fit the data very well; perhaps Eq. (38) fits a little better.

In Table 5, the limit-cycle amplitudes and periods are presented as functions of the angle of attack for the three models. The amplitude and period obtained from Eq. (39) are in very close agreement with the numerical simulation.

The results obtained from the model of Hsu and Lan give a fairly accurate estimate of the amplitude, but poorly predict the period (see Table 5). When the cubic term is added to their

model, the accuracy of the predicted amplitude decreases slightly while the accuracy of the predicted period increases. Neither set of results agrees with the numerical simulation as well as the results of Nayfeh et al.[4]

The present results suggest that the use of terms involving absolute values (e.g., $|\phi|\dot{\phi}$) does not lead to results that are as accurate as those obtained by the use of analytical terms. Also, the present results show that cubic terms are essential. Without the cubic terms divergence is not predicted. Above the critical angle of attack, the cubic terms are responsible for additional equilibria and divergence. We note that the analysis for equations such as Eq. (11) is significantly more tedious than it is for equations with only analytical terms. A constant term in the moment expression can be treated quite readily for equations having only analytical terms, whereas such a term presents analytical problems for equations such as Eq. (11).

Concluding Remarks

The analytical model of wing rock developed by Hsu and Lan has been examined. It has been shown that this model cannot predict more than one equilibrium; consequently, this model cannot predict roll divergence. It has been shown that the addition of a cubic term to the moment expression leads to additional equilibria and to the prediction of roll divergence. The results predicted by the original model of Hsu and Lan as well as those predicted by the modified model are found to be less accurate than those obtained from the model of Ref. 4.

The model of Hsu and Lan contains nonanalytical terms such as $|\phi|\dot{\phi}$, whereas the model of Ref. 4 contains only analytical terms. In the absence of a constant term in the moment equation, the analysis of the governing equation of Hsu and Lan is marginally more difficult. In the presence of a constant term, it is significantly more difficult.

Acknowledgment

This work was supported by the Air Force Office of Scientific Research under Grant 85-0158.

References

[1]Nguyen, L. T., Yip, L., and Chambers, Jr., "Self-Induced Wing Rock of Slender Delta Wings," AIAA Paper 81-1883, 1981.

[2]Levin, D. and Katz, J., "Dynamic Load Measurements with Delta Wings Undergoing Self-Induced Roll-Oscillations," AIAA Paper 83-1320, 1983.

[3]Konstadinopoulos, P., Mook, D. T., and Nayfeh, A. H., "Subsonic Wing Rock of Slender Delta Wings," *Journal of Aircraft*, Vol. 22, March 1985, pp. 223–228.

[4]Nayfeh, A. H., Elzebda, J. M., and Mook, D. T., "Influence of Pitching Motion on Subsonic Wing Rock of Slender Delta Wings," *Journal of Aircraft*, Vol. 26, June 1989, pp. 503–508.

[5]Hsu, C. and Lan, C. E., "Theory of Wing Rock," *Journal of Aircraft*, Vol. 22, Oct. 1985, pp. 920–924.

[6]Nguyen, L. T., private communication, 1988.

[7]Nayfeh, A. H., *Perturbation Methods*, Wiley-Interscience, New York, 1973.

[8]Nayfeh, A. H., *Introduction to Perturbation Techniques*, Wiley-Interscience, New York, 1981.

[9]Nayfeh, A. H. and Mook, D. T., *Nonlinear Oscillations*, Wiley-Interscience, New York, 1979.